Electronic Supplementary Material (ESI) for Reaction Chemistry & Engineering.

Supporting Information

Impact of particle-scale models on CFD-DEM simulations of biomass pyrolysis

Balivada Kusum Kumar and Himanshu Goyal*

Department of Chemical Engineering, Indian Institute of Technology Madras, Chennai, Tamil Nadu 600036, India

* E-mail: goyal@iitm.ac.in

- Section S1: Estimating the solid circulation time from CFD-DEM simulations
- Section S2: Grid convergence study for CFD-DEM simulations
- Section S3: Particle-scale grid convergence study
- Section S4: Assessment of time-averaging
- Section S5: Time-averaged intra-reactor distribution of LVG

S1 Estimating the solid circulation time

The calculation of the solid circulating time (t_c) from the CFD-DEM simulations is described here. CFD-DEM approach provides particle trajectories and helps identify the particle position at every instant. The particle location and velocity are recorded every 0.05s. Estimating the circulation time utilizing the particle positions for all the particles is extremely difficult, as the particles tend to follow random paths depending on the forces acting upon them. In this study, an approximate value of t_c is estimated by randomly selecting several particles(10s in count) and tracking their axial positions with time. A fixed particle position along the reactor height is initially identified, and the time required for the particle to circulate through the bed and reach a similar height is estimated. The average value of these circulation times is 1.4 s and is considered to be t_c. Figure S1 shows the positions of a few sand particles along the reactor height.

Next, the circulation time t_c is estimated using existing correlations available in the literature. The solid circulation time t_c is evaluated from the expanded bed height H, inlet gas velocity U, minimum fluidization velocity U_{mf}, and bubbling velocity U_b as:[1]

$$t_c = \frac{H}{0.6\,(U - U_{mf})}\left[1 - \frac{U - U_{mf}}{U_b}\right] \tag{S1}$$

The bubble velocity as a function of height (z) is estimated using:[2]

$$U_b(z) = 0.711\sqrt{g d_b(z)} + (U - U_{mf}) \tag{S2}$$

where $d_b(z)$ is the bubble diameter, g is the acceleration due to gravity, and U is the inlet gas velocity. The bubble diameter $\mathrm{d}_b(z)$ is estimated using Mori and Wen correlation:[3]

$$d_b(z) = d_{bm} - (d_{bm} - d_{b0})\,e^{-0.3z/D} \tag{S3}$$

Here d_{bm} is the bubble diameter achieved during the unconstrained coalescence in tall

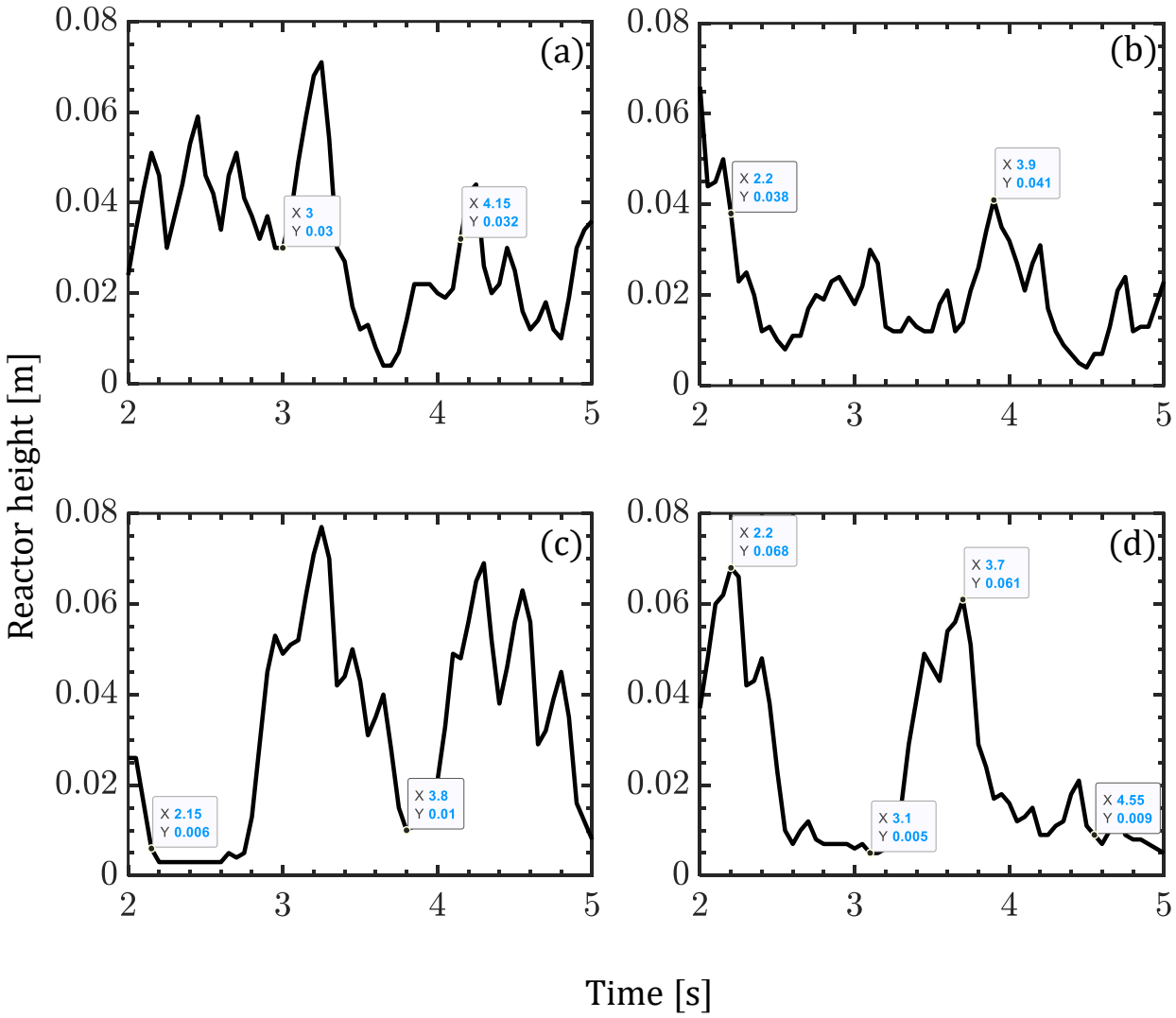

Figure S1: The axial location of four sand particles as a function of time. The labels show the reference particle positions and the corresponding time stamps used to estimate t_c.

columns estimated as

$$d_{bm} = 2.59 \left[\frac{(U - U_{mf})\, A}{g^{0.5}} \right]^{0.4} \tag{S4}$$

where A is the cross-sectional area of the bed. d_{b0} is the diameter of bubbles formed close to the distributor evaluated using:

$$d_{b0} = 1.38 \left[\frac{(U - U_{mf})\, A}{g^{0.5} N_{or}} \right]^{0.4} \tag{S5}$$

The bubble volume fraction ε_b as a function of height is given as:

$$\varepsilon_b = \left(\frac{G_b}{A} \right) / u_b(z) \approx (U - U_{mf}) / u_b(z) \tag{S6}$$

The average bubble volume fraction $(\varepsilon_b)_{av}$ can be estimated at $Z = 0.4H$, according to Fryer and Porter:[4]

$$(\varepsilon_b)_{av} = \frac{H - H_{mf}}{H} \tag{S7}$$

Equations S6 and S7 can be used to evaluate the expanded bed height H as

$$H = H_{mf} \times \frac{u_b(0.4H)}{u_b(0.4H) - (U - U_{mf})} \tag{S8}$$

Equations S2, S3, and S6 need to be iteratively solved to evaluate expanded bed height H and bubble velocity U_b. The solid circulation time t_c is estimated using Equation S1.

The solid circulating time t_c estimated using the above correlations is 0.91 s, and the corresponding expanded bed height H is 7.7 cm. The predictions from the correlations closely match with the observations from the CFD-DEM simulations, where t_c =1.4 s and H = 7.8cm.

We estimate the impact of reactor size on the time scales: solid circulation time (t_c), gas residence time (t_g), and devolatilization time (t_d). The sand bed aspect ratio (sand bed height/diameter) is maintained constant during the analysis. The bed diameter influences

the bubble diameter according to the Equations S3, S4, and S5. The bubble velocity depends on the bubble diameter as per Equation S2. The solid circulation time (t_c) is estimated as a function of the bubble velocity using Equation S1. The bed diameter is constrained to 25 cm due to the applicability of these correlation. At a constant aspect ratio, an increase in the bed height increases the gas residence time (t_g). The devolatilization time (t_d) remains the same, irrespective of the bed diameter. The variation in the time scales for increasing bed diameter is shown in Figure S2a and S2b for low and high Bi cases, respectively. At high Bi, the gas residence time, and solid circulating time are always lower than the devolatilization time, which is the case in our current study. This shows our time-scale analysis also applies to the large-scale systems at high Bi. For low Bi, $t_d > t_c$ in the present study. However, increasing the bed diameter makes $t_c > t_d$ and t_g t_d. Thus, the bed behavior could change for low Bi. More non-uniformity in the species composition in the multiphase region of the bed is expected.

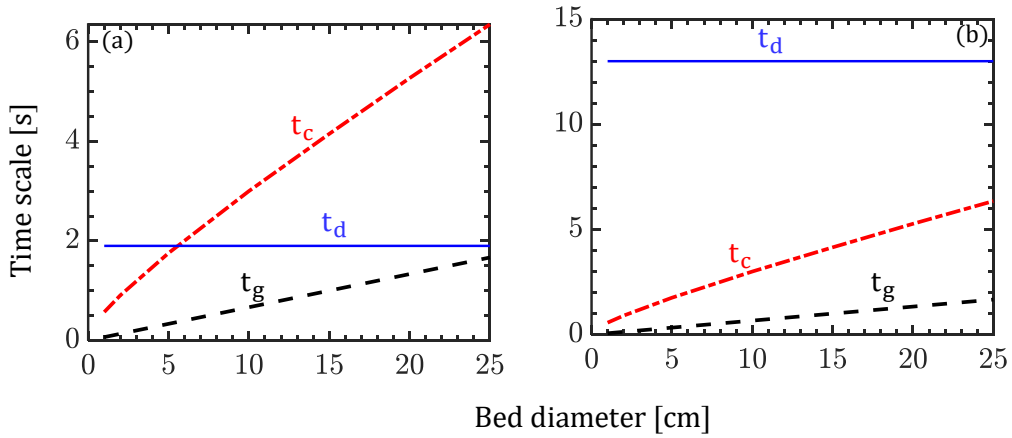

Figure S2: Influence of bed diameter on the time-scales. Solid circulation time (t_c): dash-dotted red line; Devolatilization time (t_d): solid blue line; Gas residence time (t_g): dashed black line for (a) low Bi and (b) high Bi. The sand bed aspect ratio (sand bed height/diameter) is maintained constant during the analysis.

S2 Reactor-scale grid convergence study of CFD-DEM simulations

A grid convergence study is performed to find the optimum grid size for the CFD-DEM simulations. Three grid sizes: 0.5 mm (Fine mesh), 1 mm (Normal Mesh), and 2 mm (Coarse Mesh) are considered. The grid size in CFD-DEM simulations primarily depends on the particle diameter (d_p). In general, a grid size greater than the particle diameter is implemented. Figure S2 shows the time evolution of species mass fraction at the reactor outlet for the selected grid sizes. The impact of the grid size is almost negligible in the range of grid sizes considered in this study. We use a grid size ($2d_p$) slightly greater than the maximum particle diameter (1.5mm) implemented in our CFD-DEM simulations.

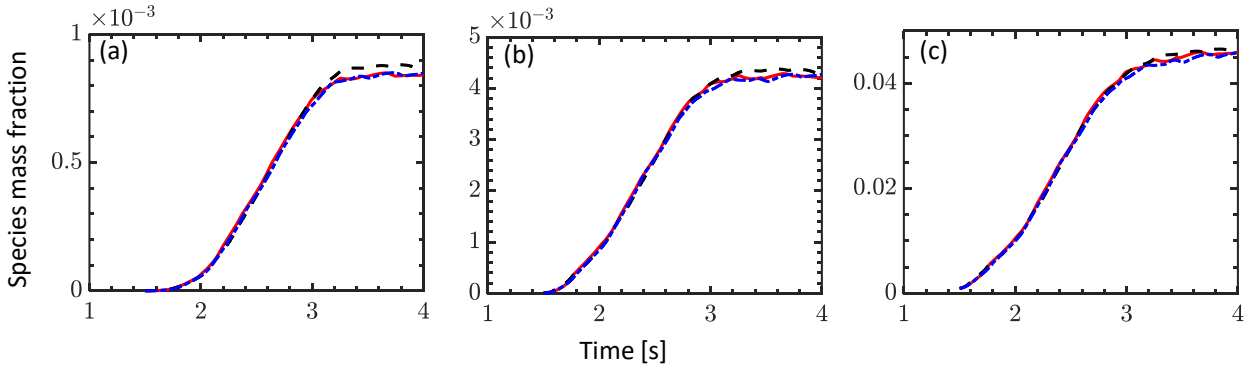

Figure S3: Grid convergence study for CFD-DEM simulations (Red solid line: coarse grid (2mm); Black dashed line: normal grid (1mm); blue dash-dotted line: fine grid (0.5 mm). (a)C11H12O4 (b) Xylose (c) H_2O.

S3 Particle-scale grid convergence study

A grid convergence study is performed at a single particle level for low and high Bi cases. The conditions experienced by the biomass particle inside a fluidized bed are imposed using an averaged heat transfer coefficients at the outer surface of the biomass particle. Table S1 provides the simulation parameters used for the grid convergence study. The number of grid points within the particle are varied from five to twenty. Figure S4 shows the grid dependence of the intraparticle model at low (top row) and high Bi (bottom row), respectively. The model predictions vary when the grid points are changed from five to ten. However, the variation in the model predictions is negligible when the number of internal grid points are varied from ten to twenty. Hence, we used twenty grid points to resolve a biomass particle in the CFD-DEM simulations.

Table S1: Parameters used in the grid convergence study for the devolatilization of a single biomass particle using the intraparticle model.

Parameter	**Value**
Biomass type	Poplar wood
Biomass composition	Cellulose : 0.4806
	Hemicellulose : 0.2611
	C-rich lignin : 0.0214
	H-rich lignin : 0.0957
	O-rich lignin : 0.1325
	Ash: .0086
Biomass particle diameter	1.5 mm ($Bi = 1.6$); 500μm ($Bi = 0.26$)
Heat transfer coefficient	295 W/m^2.K ($Bi = 1.6$); 685 W/m^2.K ($Bi = 0.26$)
Gas temperature	773 K

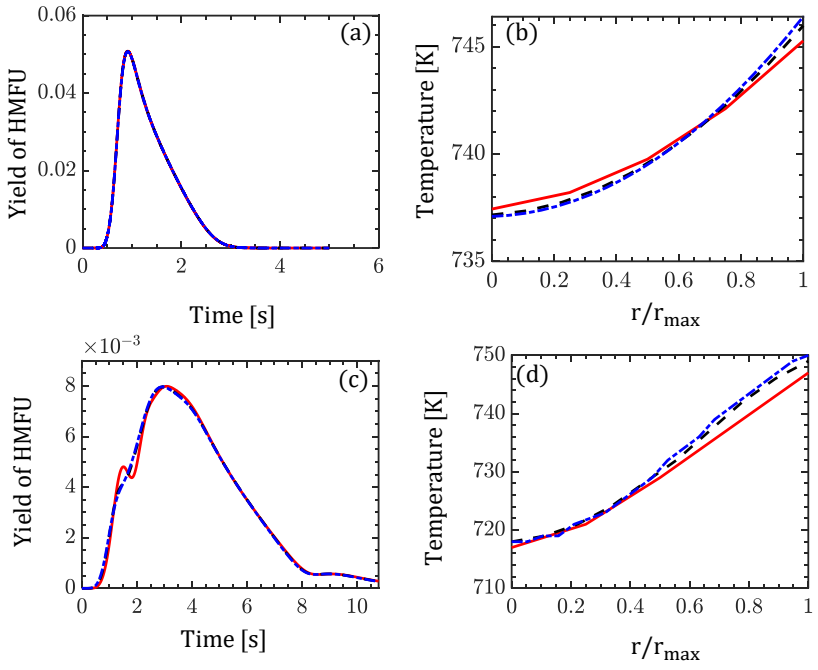

Figure S4: Grid convergence study for the intraparticle model for a single biomass particle devolatilization simulation. The transient evolution of HMFU and intraparticle temperature profile at 50% of the devolatilization time are shown for different number of internal grid points. Red solid line: 5 grid points; Black dashed line: 10 grid points; blue dash-dotted line: 20 grid points. Top row: low Bi; Bottom row: high Bi. (a, c) Transient evolution of HMFU yield; (b,d) Intraparticle temperature.

S4 Assessment of time-averaging

We assess the time period required to obtain a consistent time-averaged profile from the CFD-DEM simulations. The CFD-DEM data is averaging over a time period ranging from 1s to 5s with data files saved every 0.2s. Figures S5 (a) and (b) show the time-averaged axial profiles of LVG mass fraction obtained from the CFD-DEM simulations using the homogeneous (Fig. S5a) and intraparticle (Fig. S5b) models. The axial profiles are almost the same for a time period of 3s and above.

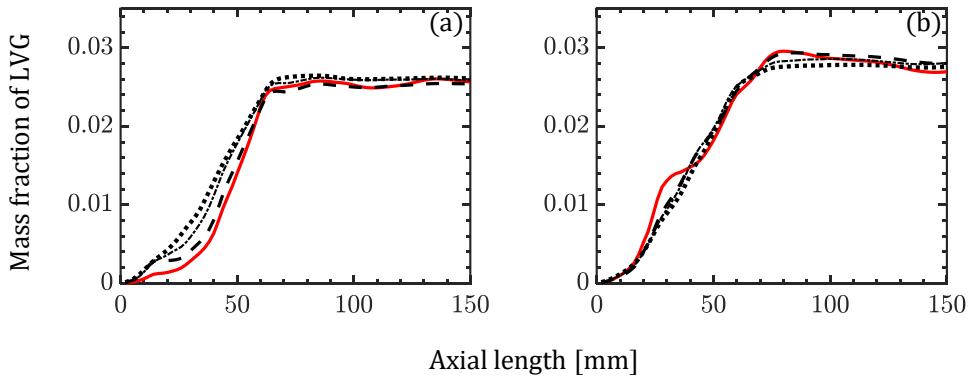

Figure S5: LVG mass fraction along the fluidized bed length averaged over the cross-section and time. The results for different periods are shown: 1s (red solid line), 2s (black dashed line), 3s (black dash-dotted line), and 4s (black dotted line) obtained from the CFD-DEM simulations using (a) homogeneous model and (b) intraparticle model.

S5 Instantaneous and time-averaged intra-reactor distribution of LVG

Plots of LVG distribution inside the reactor at various time stamps for low (Figures S6) and high Biot (Figures S7) numbers are provided here. Moreover, time-averaged plots of LVG distribution inside the reactor are provided. The top rows of Figures S6 and S7 show the LVG distribution predicted by the CFD-DEM simulations using the homogeneous model, and the bottom rows show the distributions of the CFD-DEM simulations using the intraparticle model. Significant differences are observed in the transient reactor predictions obtained from the homogeneous and intraparticle models. The time-averaging of the simulation data is performed over 3 seconds with an interval of 0.2 seconds at a statistically steady state. Figure S8 shows the time-averaged distribution of LVG inside the reactor. In contrast to the instantaneous profiles, the difference in the time-averaged profiles between the particle-scale models is negligible.

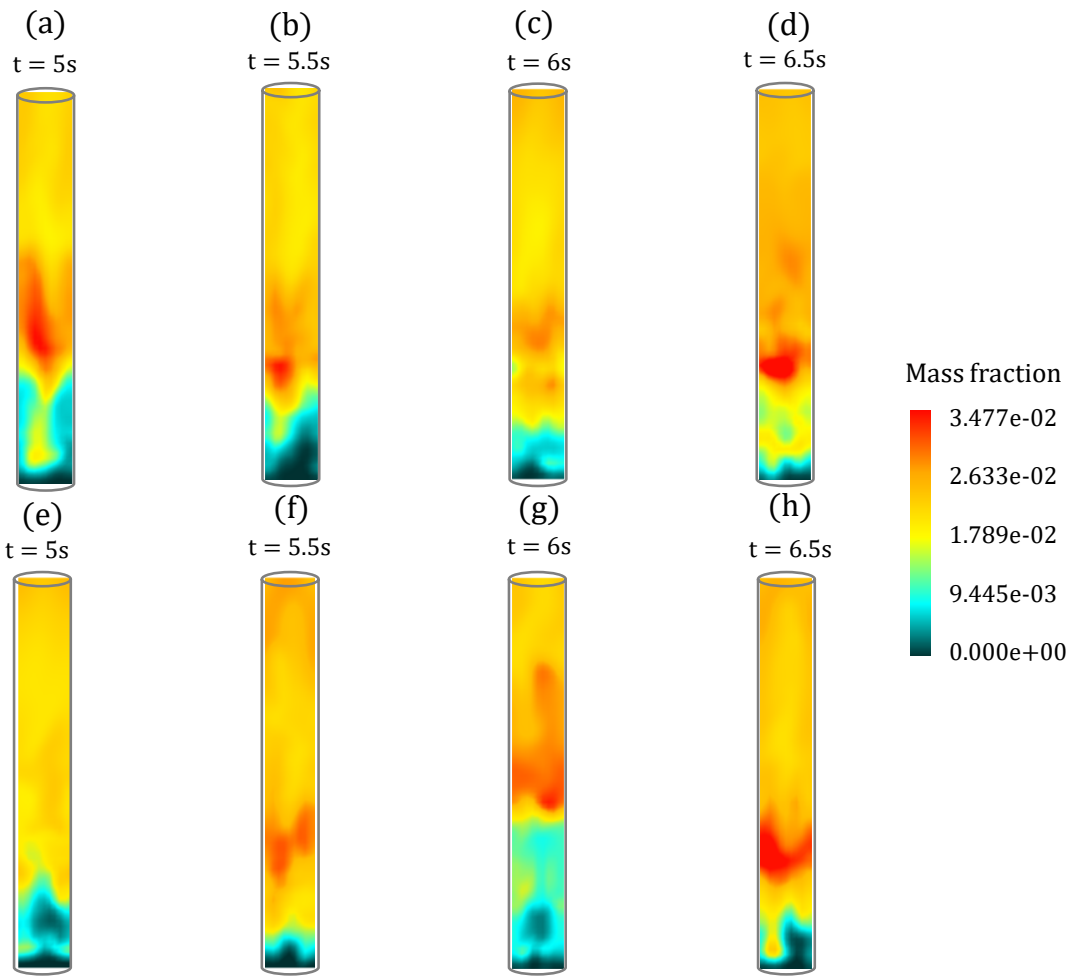

Figure S6: Instantaneous LVG mass fraction at a cross-sectional plane passing through the reactor center for low Bi. Predictions of the homogeneous model (top row) at (a) 5s (b) 5.5s (c) 6s (d) 6.5s and the intraparticle model (bottom row) (e) 5s (f) 5.5s (g) 6s (h) 6.5s.

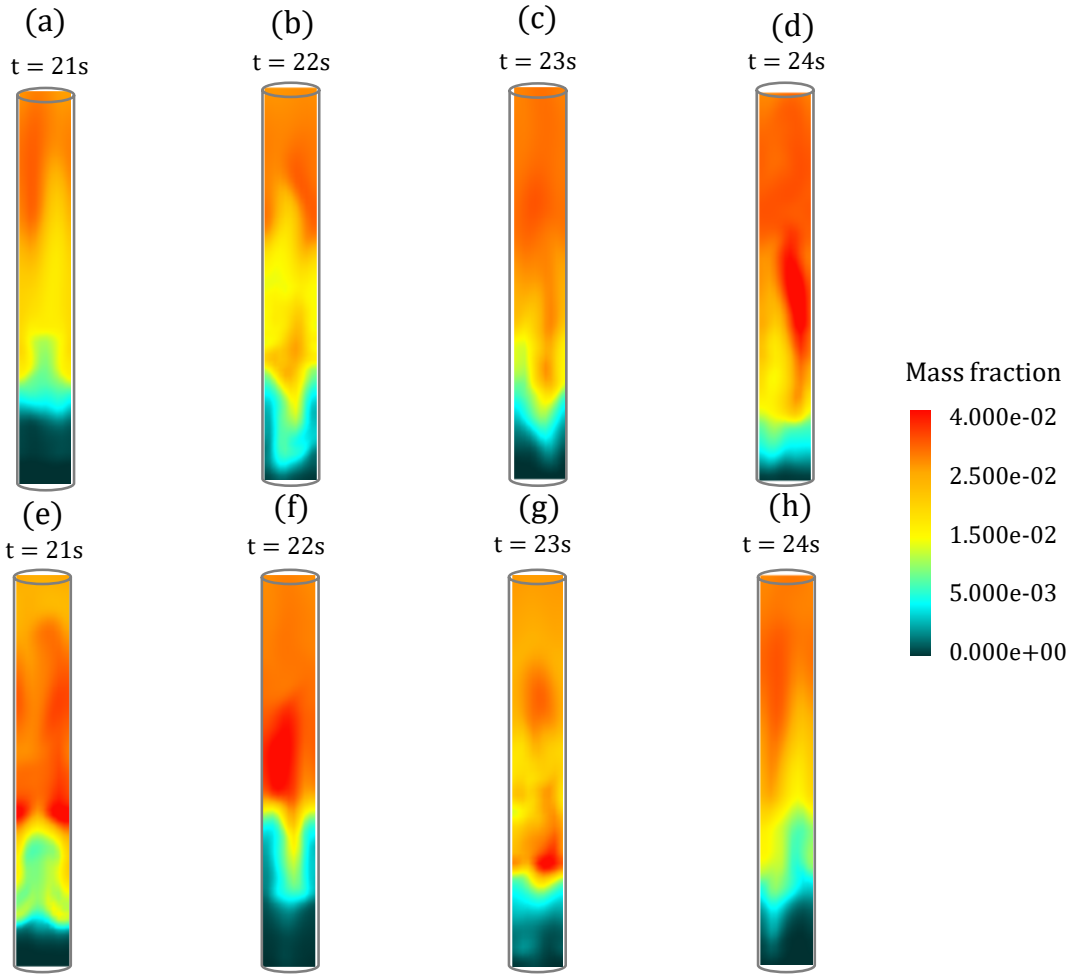

Figure S7: Instantaneous LVG mass fraction at a cross-sectional plane passing through the reactor center for high Bi. Predictions of the homogeneous model (top row) at (a) 21s (b) 22s (c) 23s (d) 24s and the intraparticle model (bottom row) at (e) 21s (f) 22s (g) 23s (h) 24s.

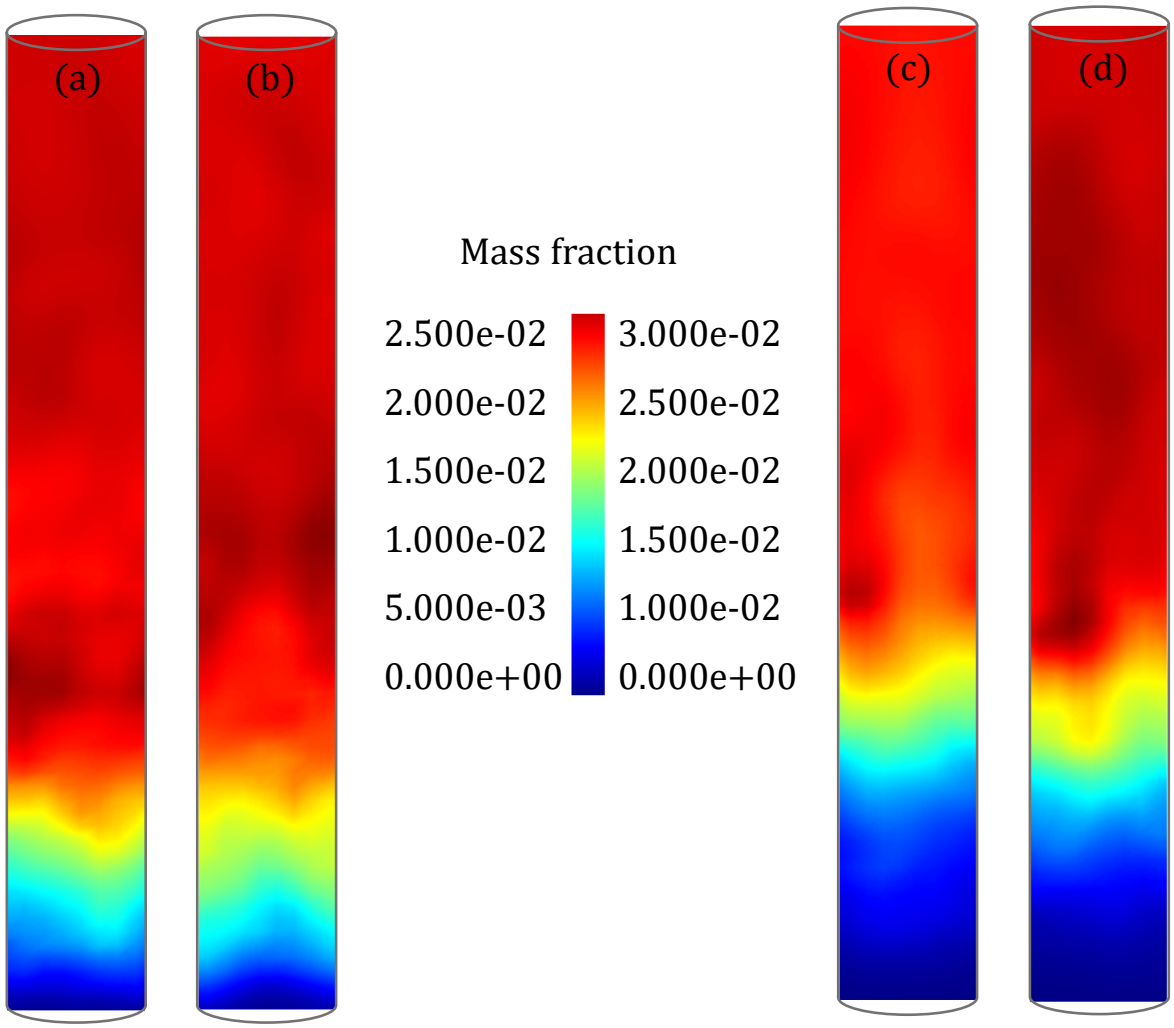

Figure S8: Time-averaged LVG mass fraction at a cross-sectional plane passing through the reactor center. Predictions of the (a) homogeneous model and (b) intraparticle model for low Bi. Predictions of the (c) homogeneous model (d) Intraparticle model for high Bi.

References

(1) Rowe, P. Estimation of solids circulation rate in a bubbling fluidised bed. *Chemical Engineering Science* **1973**, *28*, 979–980.

(2) Grace, J.; Harrison, D. The behaviour of freely bubbling fluidised beds. *Chemical Engineering Science* **1969**, *24*, 497–508.

(3) Mori, S.; Wen, C.-Y. Estimation of bubble diameter in gaseous fluidized beds. *Aiche Journal* **1975**, *21*, 109–115.

(4) Fryer, C.; Potter, O. Bubble size variation in two-phase models of fluidized bed reactors. *Powder Technology* **1972**, *6*, 317–322.